https://doi.org/10.1016/j.cemconres.2021.106669

Strength Degradation of Seawater-mixed Alite Pastes: An Explanation from Statistical Nanoindentation Perspective

Yanjie SUN, Jian-Xin LU, Chi Sun POON*

Department of Civil and Environmental Engineering,

The Hong Kong Polytechnic University, Hung Hom, Kowloon, Hong Kong

Corresponding author email: cecspoon@polyu.edu.hk

Abstract

Interest in investigating seawater concrete is increasing in recent years, but the strength degradation mechanism of seawater mixed concrete is still poorly understood. In this study, alite, the main phase in ordinary Portland cement, was hydrated with different salt solutions (NaCl, $MgCl_2$, $CaCl_2$ and simulated seawater) with a solution-to-binder ratio of 0.5, aiming to explore the effects of common cations in seawater on the micro-mechanical performance of alite pastes. Nanoindentation-energy dispersive X-ray spectroscopy analysis, porosity analysis, and phase evolution tests were carried out to reveal the microstructure of salt-added alite systems. The results showed that in addition to the acceleration of alite hydration by the salt solutions, more low-density (LD) C-S-H in the hydration products was formed. All the cations used in this study were able to enter the mesopores (2 – 5 nm) in the C-S-H particles, which contributed to improving the micro-mechanical performance of alite pastes. However, the deleterious effects of simulated seawater on the modulus and hardness of C-S-H were found, which were mainly attributed to the formation of $Mg(OH)_2$ due to the presence of Mg^{2+} in seawater.

Keywords: Seawater; Cement; Tricalcium Silicate; Hydration; Cations

1. Introduction

Concrete is the most commonly used construction material in human society as it has a variety of excellent properties such as reasonable price, high mechanical properties and robust durability, etc. [1, 2]. Within the constitutes of concrete, the mixing water is an essential component. It was estimated that about 1.5 billion tons of water was used annually for the production of concrete [3, 4]. Freshwater is the main mixing water. However, the freshwater shortage problem is increasing in some regions of the world like Middle East, North Africa and some remote islands [5-7]. According to the estimation of World Meteorological Organization (WMO), 700 million people will suffer the intense scarcity of freshwater by 2030 [8]. Thus, the possible replacement of freshwater by seawater in concrete industry has been concerned in recent years.

The application of seawater in preparing concrete can be traced back to the ancient Roman concrete sea walls built more than 2000 years ago [9]. However, with the introduction of steel bars in concrete, serious problems occurred due to the corrosive effect of seawater on steel bars [10-12]. Therefore, mixing seawater in concrete can only be applied in limited conditions, such as in plain concrete [13, 14]. The use of fiber-reinforced polymer as reinforcement has opened up renewal interest in seawater concrete. Thus, the possibility of using seawater as the mixing water is actively discussed in recent years [3].

Previous studies related to seawater concrete mainly focused on evaluating the mechanical performance, the durability and the corrosion of steel reinforcement [3, 15-19]. Most researchers agreed that the use of seawater as the mixing water could yield a higher early-age strength than that of freshwater [3, 14, 15, 20, 21], which was resulted from the accelerated hydration of seawater cement pastes [14, 22]. However, the long-term compressive strength of seawater-mixed concrete was found to decrease by 5% to 7% at 28 d compared to that of the freshwater-mixed concrete [19]. For the strength degradation caused by seawater, some explanations have been proposed. Islam et al. attributed the strength reduction to the leaching of hydration products [23]. Wegian et al. suggested that the lower long-term mechanical performance was the result of salt crystallization and expansion of $Mg(OH)_2$ and $CaSO_4 \cdot 2H_2O$ [19]. Zhang et al. [24]

suggested that the formation of Friedel's salt and a lower polymerization of the hydration products were two main causes for the strength degradation. But, up to now, limited research tried to explain the strength degradation from the perspective of micro-mechanical property evolution of hydration products in the seawater concrete.

Nanoindentation is an effective and powerful tool to explore the micro-mechanical properties of solid materials and has been applied in cement and concrete studies [25-28]. According to previous nanoindentation studies on cement pastes, the main hydration product in cement pastes, namely calcium silicate hydrates (C-S-H), can be divided into low-density (LD) C-S-H and high-density (HD) C-S-H based on their intrinsic properties (Er: modulus and H: hardness) [29]. These two C-S-H phases have significant influences on the overall mechanical performance of the cement pastes.

Seawater is a complex system with a variety of inorganic and organic phases, and chloride is the most abundant element. Chloride ion is known to be the main contributor for the accelerated hydration of cement [30, 31]. Apart from chloride ion, other major ions in seawater are Na^+, Mg^{2+} and Ca^{2+}. The early research on the effects of common cations in seawater on the hydration of cement was conducted by Edwards at al. [32], and the accelerating effects of these cations were ranked as $Ca^{2+} > Mg^{2+} > Na^+ > H_2O$. The research by Kondo et al. came up with a similar result and attributed it to the mobility of the ions. However, there is no direct research on comparing the effects of these cations on the hydration of cement.

This study adopted the nanoindentation technique to study the effects of common cations in seawater on the micro-mechanical properties of cement pastes, with a view to revealing the underlying meahcnisms of the strength degradation by using seawater in preparing concrete. A subsystem was used to simplify the complex compositions of ordinary Portland cement and seawater by mixing single salt solutions in the seawater with alite (major clinker phase in ordinary Portland cement).

2. Materials and methods

2.1 Materials and sample preparation

The alite used in this study was synthesized in the laboratory by calcium carbonate

and silica fume, following the method by Li et al. [33] The synthesized alite was characterized, and the details are shown in Fig.1. The crystalline phases of the sample were analyzed by X-ray Diffraction (Rigaku Smartlab, Japan) with Rietveld refinement method. The results showed that the purity of alite was about 94.1 wt.% and the remaining phase was β-C_2S. Fig. 1b shows the particle size distribution of the alite powder measured on a Malvern MS3000 laser particle analyzer. The average particle size was 16.9 μm.

AR grade NaCl (NC), $MgCl_2$ (MC), $CaCl_2$ (CC) were used to prepare the salt solutions with the same concentration at 0.42 mol/L to compare the effects of the different cations. Simulated seawater (SW) was prepared according to ASTM S-98 (2013), and its composition is shown in Table 1. The concentration of NaCl in SW was also 0.42 mol/L.

Alite was mixed with deionized water (DI), NC, MC, CC and SW solutions at the same solution-to-binder ratio of 0.5. The pastes were sealed in plastic membranes and kept at 25 ± 2°C. At 1 d and 28 d, the pastes were demolded and analyzed with a variety of characterization techniques.

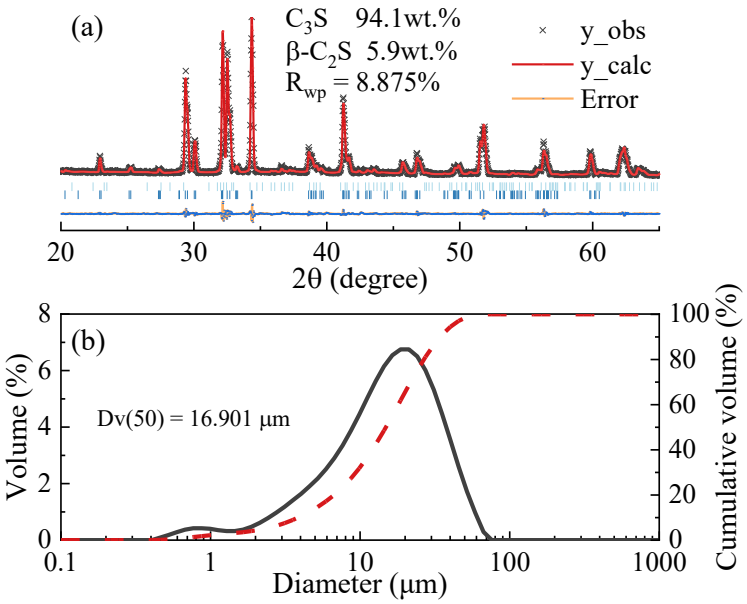

Fig. 1 (a)Crystalline phase composition by Rietveld analysis and (b) Particle size distribution of the synthesized alite.

Table 1 Chemical compositions of simulated seawater

Component	NaCl	$MgCl_2$	Na_2SO_4	$CaCl_2$	KCl	$NaHCO_3$	KBr
Concentration (g/L)	24.53	5.20	4.09	1.16	0.695	0.201	0.101

2.2 **Characterization techniques**

For the nanoindentation test, the samples were first mounted into epoxy in a vacuum environment for 1d before polishing. To obtain a smooth surface, the samples were first coarsely polished with polishing papers (180, 240, 600, 800 and 1200 grit). Because of the hydration characteristics of C_3S, ethanol was used instead of water as the polishing fluid. After the coarse polishing process, the fine polishing process was conducted on polishing papers (3, 1 and 0.25 μm) with corresponding oil-based diamond suspensions for 30 min per paper. Finally, the samples were cleaned in an ethanol bath by ultrasond for 30 min to remove debris and suspension on the surface. After these procedures, the RMS roughness of samples was examined by Scanning probe microscopy (SPM) as shown in Fig. 2, and the average RMS for all samples were less than 30 nm over a 100 μm^2 area. It met the standard that the average RMS was less than 1/5 of the average indentation depth (300 nm) over the 200 times the average indentation depth (60 μm) [34]. After the examination of the surface, The micro-mechanical properties were characterized on a Nano-indenter (Hysitron TI Premier, Bruker) equipped with a three-sided pyramid Berkovich tip. Before testing, the equipment was calibrated on the standard fused quartz sample.

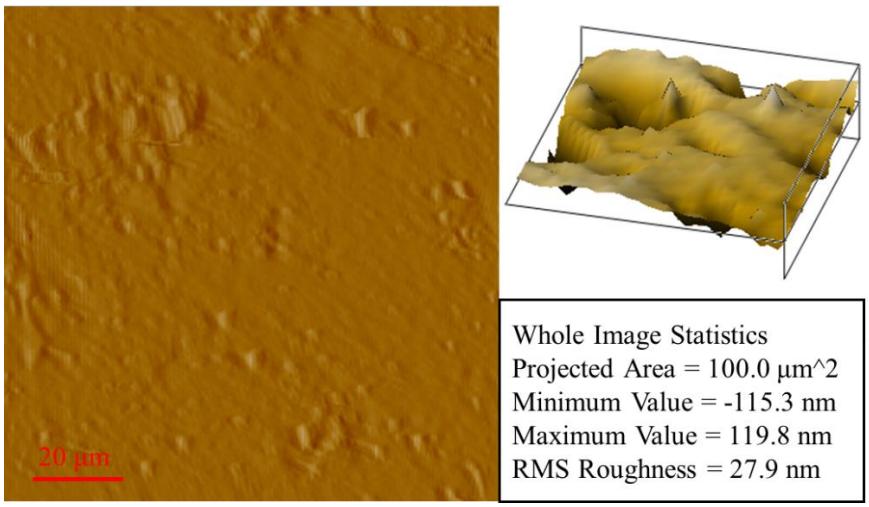

Fig. 2 SPM and 3D plotting of the polished surface

The trapezoidal loading function adopted in this study is shown in Fig. 3a, the maximum loading (2000 µN) was reached at 10 s and hold for 5 s, then the unloading was finished in 10 s. From the typical load-depth curve (Fig. 3b), two micro-mechanical parameters can be obtained, indentation modulus (M) and hardness (H) [29]. 10 × 10 grids with the grid spacing of 10 µm (Fig. 3c) were applied for each area and the surface after indentation is shown in Fig. 3d. For each sample, three distinct areas were selected, so 300 data points were collected for each sample.

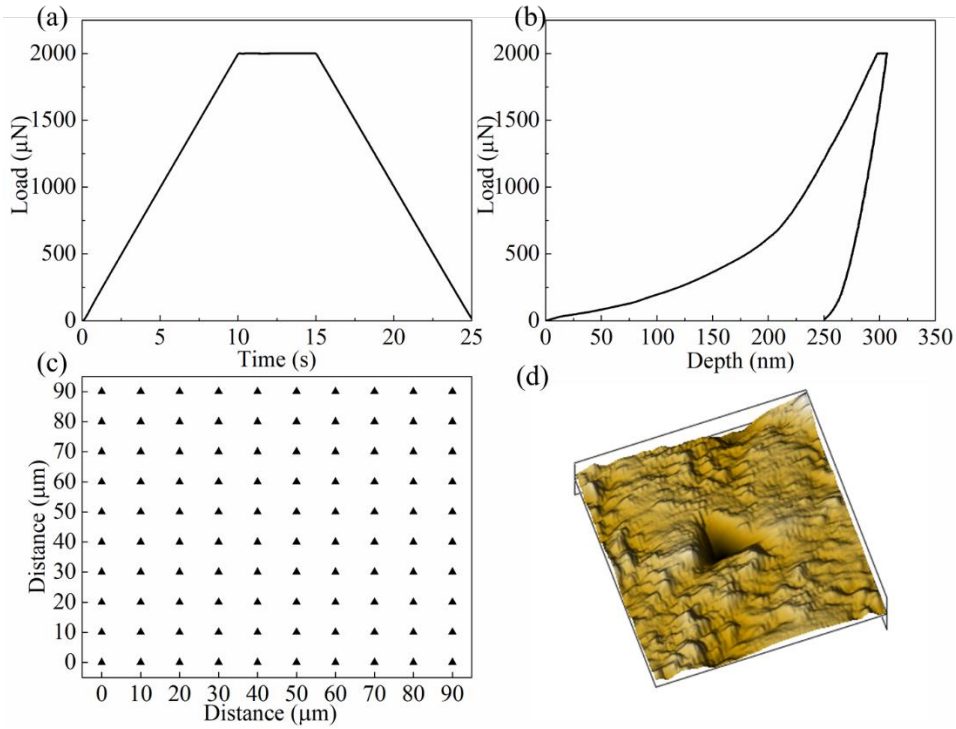

Fig. 3 (a) The loading function for nanoindentation; (b) A typical load-depth curve of the nanoindentation test; (c) Grid technique arrangement; (d) A representative surface indented.

The elemental composition of the hydration products was characterized by a Field emission scanning electron microscope (FESEM, MAIA3, Tescan) equipped with an energy dispersive X-ray spectroscopy (EDX, Essence, Oxford) detector. The EDX testing was conducted in the same area for the nanoindentation test, and 100 data points were collected. The testing condition was controlled at the accelerating voltage of 20 kV and the magnification of 2000×. For each point, the dwell time was 60 s. The compositional data were then correlated with the micro-mechanical results to elucidate the mechanical property change of the alite pastes due to the addition of the salt solutions.

The ASAP 2020 Micromeritics Accelerated Surface Area and Porosimetry instrument was used to examine the pore distribution of the hydration products. The bath temperature was −196 °C. The sample powders were firstly preheated at 60 °C for 24 hours. Nitrogen adsorption and desorption data were collected and further analyzed by Barrett-Joyner-Halenda (BJH) analysis to obtain the pore size distribution.

Thermogravimetric analysis (TGA, Rigaku Thermo Plus EVO2) was used to

characterize the portlandite and total combined water contents of the hydrated solid powder samples. The heating was programmed to start at 30 ℃ and end at 1000 ℃ with a heating rate of 10 ℃/min. The tangent method was adopted to quantify the phase compositions [35]. For X-ray diffraction analysis (XRD Rigaku Smartlab), the measurement was operated under the Bragg-Brentano geometry mode at 40 kV and 30 mA. The data collection range was 7° - 70° 2θ for CuKα radiation with a step size of 0.02° (0.5 s for each step). After collecting the data, the Rietveld method was used to quantify the phase compositions of the hydration products. Transmission electron microscope (TEM, JEOL Model JEM-2100) was used to observe the morphology of hydration products. Before the TEM experiment, the hydrated alite samples were first ground into a powder and then immersed in ethanol. Ultrasonic dispersion was used as a pre-treatment. 1 mL of the suspension liquid was transferred on a carbon microgrid support membrane. Then, the morphologies of hydration products were characterized. At the same time, EDX measurement was used to analyze the elemental compositions. ^{29}Si nuclei was scanned on a JEOL ECZ 500 MHZ solid-state NMR spectrometer. More than 2000 scans were conducted before getting the spectra.

3. Results

3.1 Homogenized Micro-mechanical Properties

The homogenized micro-mechanical properties provide an estimation of the global micro-properties of the alite pastes. It depends on the contributions of each phase in the matrix (i.e., a high percentage of hard phases increases the total hardness). Based on the studies of Vandamme et al. [36] and Wilson et al. [37], the homogenized modulus Er_{hom} and hardness H_{hom} of a composite can be estimated using the Reuss bound, and the Voigt bound (uniform strain) as indicated in (1) and (2), assuming an identical Poisson's ratio for the N nanoindentation measurements randomly distributed in the material. The homogenized properties were obtained from the average of the bounds.

$$\left(\frac{1}{N}\sum_{i=0}^{N}\frac{1}{Er_i}\right)^{-1} \leq Er_{hom} \leq \frac{1}{N}\sum_{i=0}^{N} Er_i \quad (1)$$

$$\min_{N} H_i \leq H_{hom} \leq \frac{1}{N}\sum_{i=0}^{N} H_i \quad (2)$$

As shown in Fig. 4, both the homogenized modulus and hardness of the DI samples increased from 1 d to 28 d. This was due to the continuous hydration of alite, and more C-S-H was formed in the matrix, which would densify the microstructure of alite pastes However, the mechanical performance of the salt-added samples showed a different trend. At 1 d, the modulus and hardness of all salt-added samples were higher than those of DI samples. When CC solution was used as the mixing water, the alite pastes had the best micro-mechanical performance at 1 d. The homogenized modulus and hardness of the alite pastes mixed with CC were increased by 29% and 84% respectively compared to those of the DI group. That was due to the strong acceleration effect of CC, which is a common acceleration admixture used in concrete preparation [38, 39]. But at 28 d, the results diverged when compared to the DI sample. With the incorporation of NC and CC, the modulus and hardness were still higher than that of DI samples. While MC and SW had negative effects on the overall properties. This suggests that Mg^{2+} in SW would have a prominent influence on the micro-mechanical properties of alite pastesThe differences in micro-mechanical properties were associated with the varying fundamental properties of C-S-H, the percentage of each phase present and the porosity of the alite pastes. These influencing factors are further discussed in the following sections.

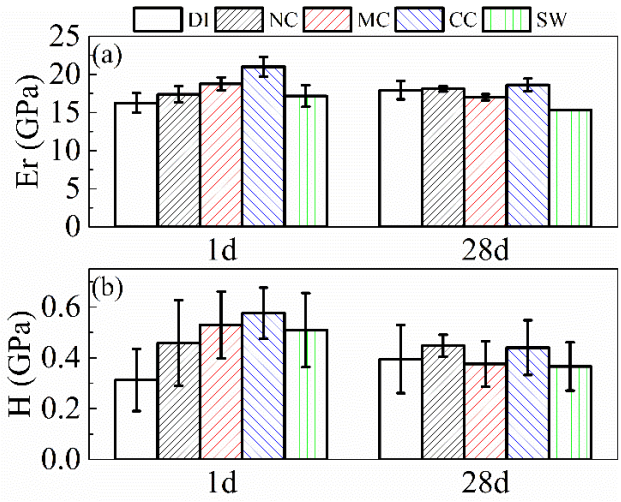

Fig. 4 Homogenized mechanical properties for (a) the indentation modulus Er and (b) the indentation hardness H.

3.2 Coupled chemo- micro-mechanical statistical analysis

The combination of Grid nanoindentation and elemental distribution (EDX) techniques was a common method to study heterogenous composite materials [40]. Based on a large number of test data, a multivariate cluster modeling approach was introduced to process these data. Statistical cluster analysis was based on the maximum likelihood estimation [41]. The micro-mechanical property distribution of the alite pastes was assumed as a Gaussian Mixture Model (GMM). Each phase in the alite pastes was treated as two-dimensional Gaussian distribution. Fig. 5a shows the representative cluster analysis results, which were grouped into four phases, viz Low Density (LD) C-S-H, High Density (HD) C-S-H, $Ca(OH)_2$ (CH) and anhydrous alite. The average modulus and hardness of each phase were calculated according to the multivariate cluster analysis results. Together with the nanoindentation tests, EDX measurement was also conducted at the same region of the samples, and the multivariate cluster analysis technique as mentioned above was also used to analyze the EDX data as shown in Fig. 5b. The dimensions for EDX analysis are oxide total (the mass content of oxide) and Ca/Si ratio. Before the cluster analysis, data with $Ca/Si \geq 3$ were separated and grouped as a mixture of alite and CH. The remaining data were divided into two phases: LD C-S-H and HD C-S-H. With the EDX data, the average Ca/Si ratio and the water content for each phase can be obtained.

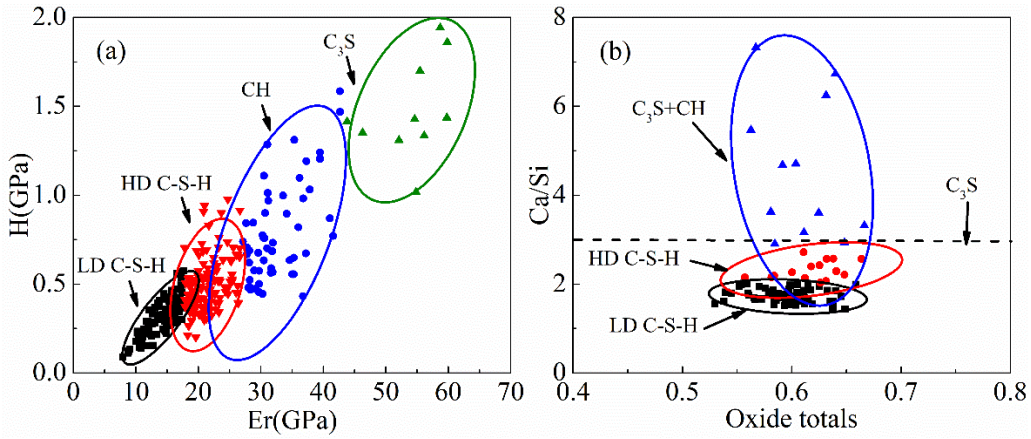

Fig. 5 Cluster analysis of alite pastes for (a) the indentation modulus Er versus the indentation hardness H; (b) Oxide totals versus Ca/Si ratio.

The percentages of each phase present were calculated according to the statistical analysis of the test results are showed in Fig. 6. At 1 d, there were still alite in the DI, NC and MC samples, while no anhydrous phase was detected in CC and SW. That indicated the stronger accelerating effect of the latter group of salts. Also, in the process of hydration, the amount of LD C-S-H continuously increased, especially for the samples prepared with MC and SW, and all C-S-H phase detected was LD C-S-H at 28 d. This is consistent with the homogenized analyses that the final homogenized modulus and hardness for MC and SW were lower than that of the DI reference group. As for the samples mixed with NC and CC, the percentage of HD C-S-H was higher than that of DI, the final homogenized micro-mechanical performance was thus improved. The percentage change also indicated that the LD C-S-H was produced not only from the hydration of alite, but also from the transformation of HD C-S-H. The CH and alite content detected by nanoindentation analysis was found to be lower than that detected by other methods, like XRD and TG. This was because part of CH and alite was intermixed with C-S-H [25].

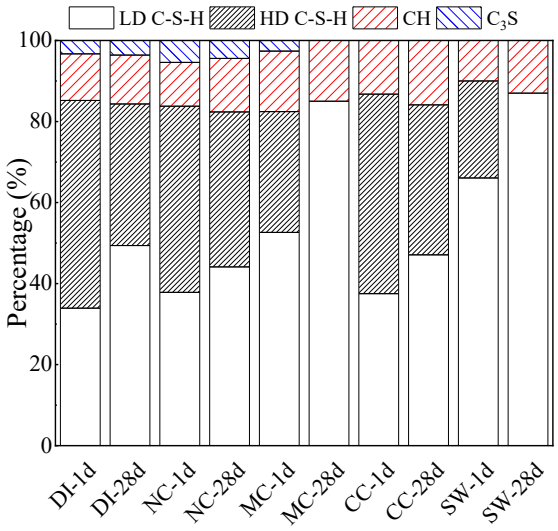

Fig. 6 Percentages of phases calculated according to nanoindentation analysis.

The cluster analysis of the micro-mechanical performance of each group at 1 d and 28 d are concluded in Fig. 7. For DI sample, the modulus of LD C-S-H was increased from 14.3 GPa to 15.4 GPa between 1 d and 28 d. The variation for hardness also showed a similar trend. This indicated that with the hydration of alite in DI water, both the micro-mechanical performance and percentage of LD C-S-H continually increased. This reinforcement of the LD C-S-H contributed to the homogenized micro-mechanical property enhancement of the alite pastes from 1 d to 28 d. The modulus and hardness of LD C-S-H for the other groups show similar trends with DI from 1 d to 28 d. On the contrary, the modulus of HD C-S-H in DI sample was reduced from 19.9 GPa to 19.0 GPa, and similar changes were found in other groups. In MC and SW samples, no HD C-S-H were detected at 28 d. This trend demonstrated that with the hydration of alite pastes, the percentage and the micro-mechanical properties of LD C-S-H were steadily improved at the expense of the decomposition of HD C-S-H. With the incorporation of MC and SW, this decomposition process was significantly accelerated.

At 1 d, the addition of NC increased both the modulus and hardness of LD C-S-H by 9% and 30% respectively compared to the reference group. Similarly, these two properties were enhanced by 33% and 46% due to the presence of CC. On the contrary, both MC and SW had deleterious effects on the micro-mechanical properties of LD and HD C-S-H. This suggests that SW and Mg^{2+} had a key degrading influence on the LD

C-S-H. At 28 d, the additions of NC and CC still reinforced both LD C-S-H and HD C-S-H. HD C-S-H decomposed completely in MC and SW, indicating that the incorporation of Mg^{2+} in mixing water contributed to the transformation from HD C-S-H to LD C-S-H.

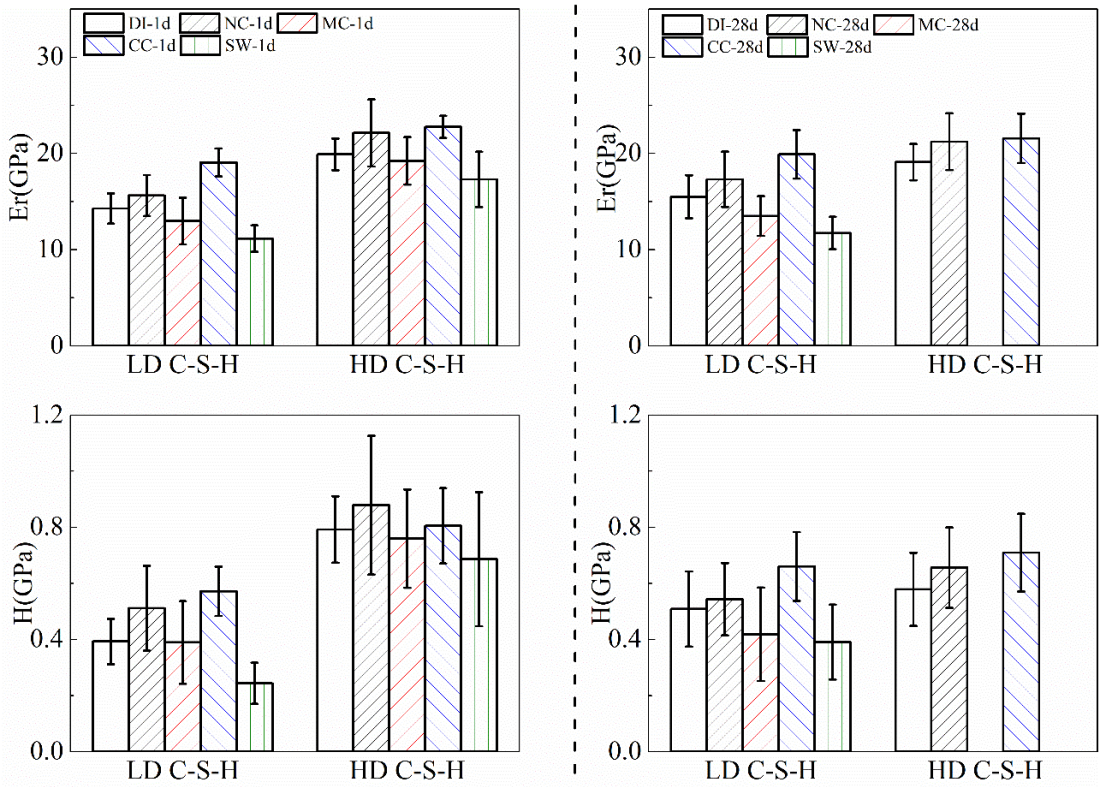

Fig. 7 The modulus and hardness for samples at 1 d and 28 d.

The H_2O content within C-S-H ((includes liquid water trapped in the nanopores of C-S-H [42])) can be obtained based on the total values of oxide [25]. Similar to cluster analysis as mentioned above, the The Ca/Si ratio and the number of H_2O molecules combined with LD C-S-H and HD C-S-H were calculated and the results are shown in Fig. 8. For DI sample, the average Ca/Si ratio of LD C-S-H was increased from 1.85 to 1.93 between 1 d and 28 d, while the average Ca/Si ratio of HD C-S-H was decreased from 2.50 to 2.36. For other samples, a similar trend was observed, with the progress of hydration of alite, the Ca/Si ratio would increase for LD C-S-H and decrease for HD C-S-H. These results indicated that calcium was continuously leached out from HD C-S-H and LD C-S-H was enriched by calcium during the hydration. H_2O molecules were

mainly present in mesopores of the C-S-H particles [43]. The ions in the salt solutions would enter the mesopores and substitute part of the H_2O molecules [44]. The change of H_2O molecule present can thus be an index for the ion substitution. For the reference system, the number of H_2O molecules combining on the C-S-H of LD C-S-H at 1 d was 3.59 and the value was reduced to 3.36 at 28 d. Similarly, the corresponding value for HD C-S-H was also decreased. At 1 d, the addition of NC had no apparent influence on the Ca/Si ratio of both LD C-S-H and HD C-S-H, but the combined H_2O content was decreased from 3.59 ± 0.67 to 3.37 ± 0.38 as compared to the reference system. At 28 d, the trend was similar for NC added samples. The results indicated that the addition of Na^+ mainly affected the mesopores of C-S-H particles, which would be further discussed in section 3.3. As for the incorporation of CC, The Ca/Si ratio of LD C-S-H and HD C-S-H both showed an increase compared with the DI group. The extra calcium content is the consequence of a deprotonation of the silanol groups in C-S-H [45]. Also, the excessive Ca^{2+} would also substitute part of H_2O in C-S-H particles, inducing the decrease of combined H_2O. The Ca/Si ratios of C-S-H in MC and SW groups were found to be lower than that of the reference system at 1 d. And at 28 d, all HD C-S-H disappeared in these two systems. This discalcification effect was due to the formation of M-S-H in the alite pastes with the prenence of Mg^{2+} [46, 47], which would compete with Ca^{2+} on the combination of silicate ions. According to the combined H_2O analysis, the Mg^{2+} also replaced H_2O molecules in C-S-H.

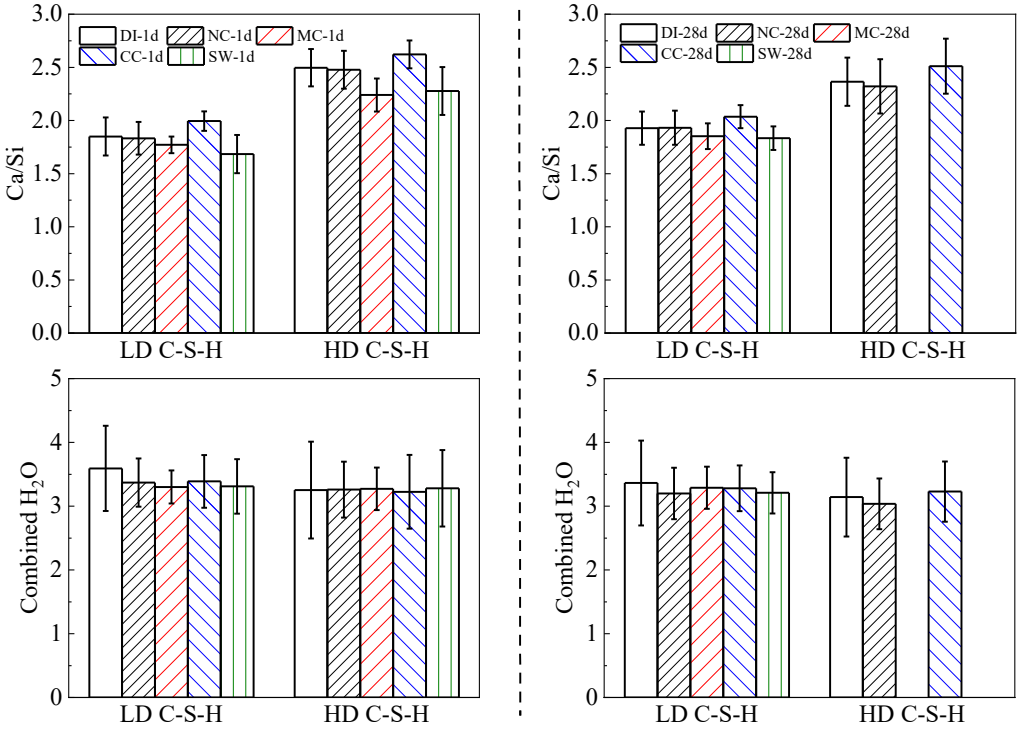

Fig. 8 The Ca/Si ratio and combined H_2O of C-S-H in samples at 1 d and 28 d

3.3 Pore size distribution analysis

The pore size distribution was analyzed using Barret-Joyner-Halenda (BJH) method [48], which is suitable for the analysis of mesopores (2 nm to 50 nm). The details of the analysis results are shown in Fig. 9. Generally, the main pore network lied in the range of 2 nm to 5 nm [49], corresponding to the pores between C-S-H chains. With the addition of NC, the pore volume at this range decreased noticeably compared to that of DI group. Larger pores (5 nm to 50 nm), which corresponded to the pores between C-S-H particles, of the NC sample also decreased. The addition of CC had a similar effect on the pore distribution of alite pastes. These results were consistent with the improved micro-mechanical properties of alite pastes by the addition of NC and CC. A second maximum of the pore size distribution curves was observed in MC and SW pastes in the range of 5 nm to 50 nm, which indicated that the addition of Mg^{2+} contributed to the formation of more coarse pores, and as a result, the micro-mechanical properties degraded. The degradation mechanism would be further discussed in the next section.

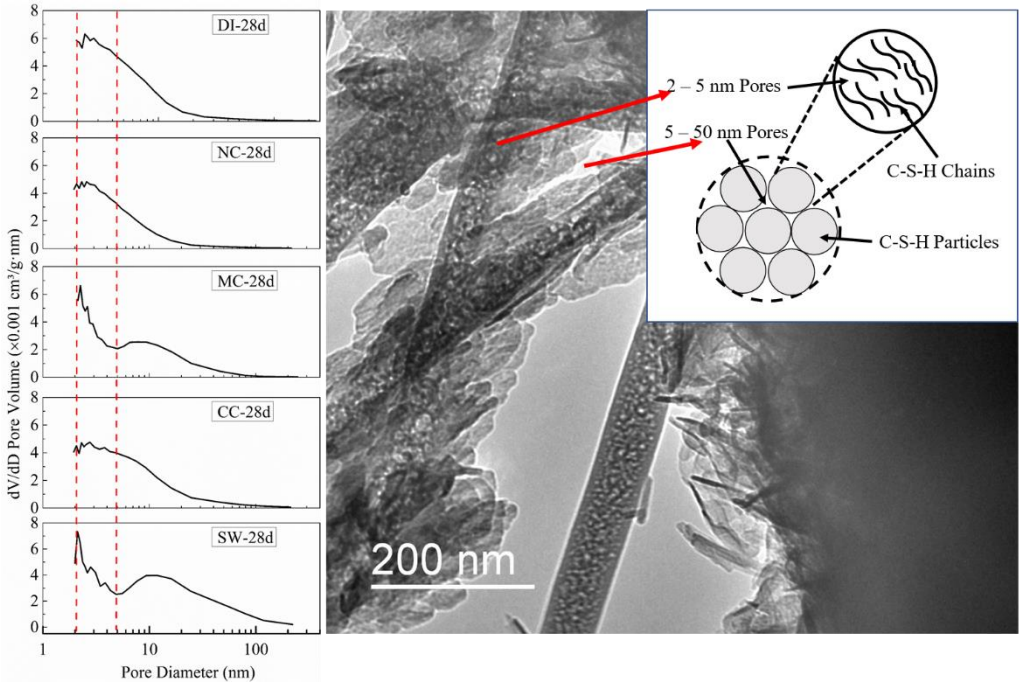

Fig. 9 BJH adsorption dV/dD pore volume analysis of each samples at 28 d.

3.4 Phase evolution with the addition of Mg^{2+}

Mg^{2+} was noticed to have a prominent degradation effect on the micro-mechanical of alite pastes. Thus, the phase development of hydration products of MC system was further studied. The XRD and DTG results (Fig. 10) show that at 1 d, $Mg(OH)_2$ can be detected. However, as the hydration of alite pastes progressed, $Mg(OH)_2$ disappeared or decreased to a tiny amount, which was not identified by XRD and TG at 28 d. This was due to the dissolution of brucite and the formation of M-S-H [47]. The morphology test results (Fig. 11) also support this mechanism, that at the initial hydration period, the C-S-H fibers were surrounded by a mixture of $Mg(OH)_2$ and $Ca(OH)_2$, and these fluffy crystalline phases filled the pores among C-S-H particles. While, at 28 d, $Mg(OH)_2$ was decomposed, leaving a large volume of pores among the C-S-H particles, which were thought to have negative effect on the micro-mechanical performance of C-S-H.

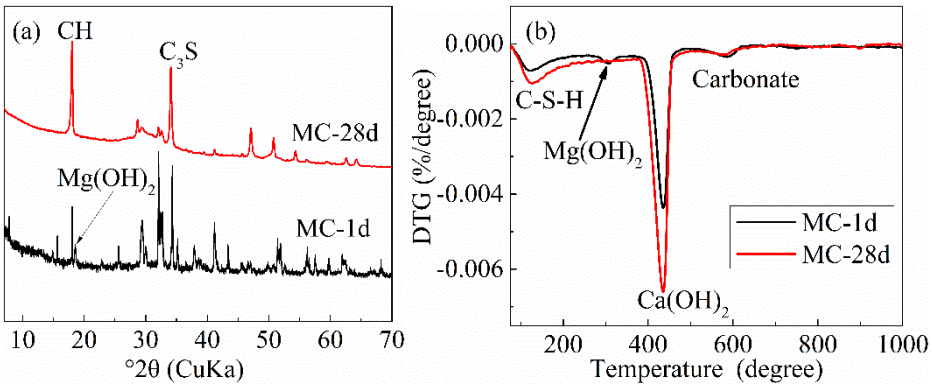

Fig. 10 XRD and DTG analysis of alite pastes mixed with MC.

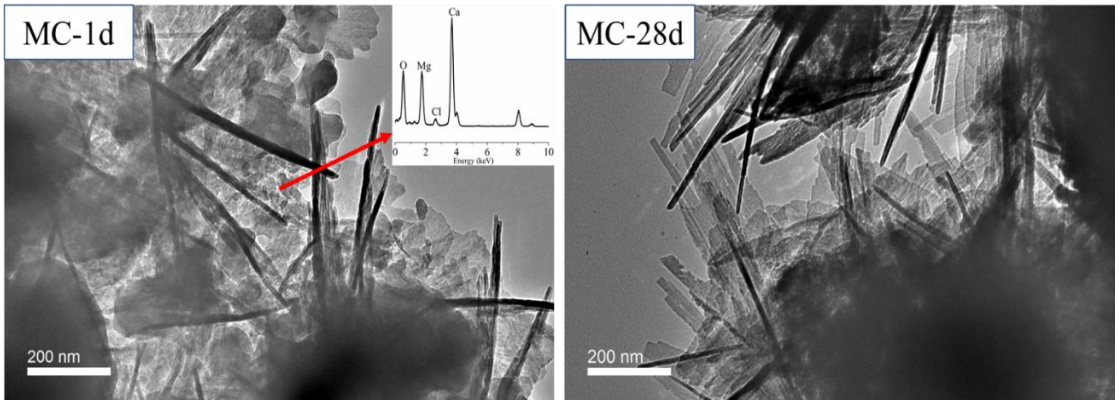

Fig. 11 The decomposing process of $Mg(OH)_2$ in MC- alite paste

4. Discussion

The SW-blended alite pastes were found to obtain a degraded micro-mechanical property compared with the one mixed with DI water. To exploit the mechanism for the degradation phenomenon, the common inorganic chloride salts were mixed with alite separately to compare the effects of different cations. The EDX analysis showed that there was no obvious decalcification effect by Na^+. It mainly entered into the pores between C-S-H chains (2 – 5 nm) and the pores between C-S-H particles (5 – 50 nm) as illustrated in Fig. 9. With this filling effect, the modulus and hardness of C-S-H was improved. Furthermore, this contributed to the overall improvement of the mechanical properties of alite paste. Since the principal role of Na^+ was a filler, the Ca/Si ratio of C-S-H in the NC group has no noticeable change compared to the reference group. The addition of excess Ca^{2+} was also found to enhance the micro-mechanical properties of alite pastes. Different from the effect of Na^+, excessive Ca^{2+} addition increased the

Ca/Si ratio of both LD C-S-H and HD C-S-H, which contributed to a more compact C-S-H structure.

The effects of Mg^{2+} can be divided into two aspects. Firstly, the filling function similar to Na^{+} as elucidated above. That was evidenced by the decrease of porosity at the range of 2 nm to 5 nm as compared with the reference system. This improved the micro-mechanical performance of the alite pastes. And also, the bounding water in C-S-H was decreased due to the replacement of water by Mg^{2+}. However, according to the nanoindentation test results, the final paste strength decreased with the addition of MC. This was due to the second effect of Mg^{2+}. When alite was mixed with MC solution, a large amount of fluffy $Mg(OH)_2$ crystals were formed quickly. These $Mg(OH)_2$ would intermixed with the C-S-H fibers and occupied a lot of space, due to its expansive properties [50]. But, as $Mg(OH)_2$ tended to decompose and more M-S-H was formed as the hydration progressed [51], pores were left within the particles of C-S-H. That induced the increase of the porosity in the rage from 5 nm to 50 nm. As a result, the homogenized modulus and hardness of MC pastes were lower than that of the reference group. The incorporation of Mg^{2+} also contribute to the decalcification of both LD C-S-H and HD C-S-H, as the Mg^{2+} would combine with silicate ions to form M-S-H. Therefore, the leaching of Ca^{2+} from C-S-H also cause the degradation of C-S-H.

Therefore, the different cations in seawater had distinct impacts on the hydration products of alite. Overall, the Mg^{2+} has a dominant deleterious effect on the micro-mechanical properties of alite pastes, especially on the properties of C-S-H. However, the incorporation of the concerned cations contributed to the filling effect, which improved the mechanical performance.

Conclusion

Alite was mixed with DI water and four soluble solutions (NC, MC, CC, SW) to understand the effects of different cations in seawater on the hydration of alite. Based on the results, the following conclusions can be drawn:

- The addition of SW would contribute the degradation of alite pastes. The deleterious effect of SW on the alite hydration products was mainly attributed to

the effects of Mg^{2+}.

- All the studied cations could an enter the mesopores (2 – 50 nm) in C-S-H particles and act as fillers, which increased the micro-mechanical properties of C-S-H and hydrated alite pastes.
- Mg^{2+} reacted with OH^- to form $Mg(OH)_2$ initially, which was continuously decomposed as the hydration progressed . The decomposition left space for LD C-S-H to form and generated more pores among C-S-H particles, which decreased the modulus and hardness of the alite pastes.

Acknowledgement

The work described in this paper was supported by the Theme Based Research Scheme of the Research Grants Council of the Hong Kong SAR Government (Project No. T22-502/18-R).

References

[1] A.M. Neville, Properties of concrete. Vol. 4. 1995: Longman London.
[2] S.L. Wood, Evaluation of the long-term properties of concrete. 1992: Portland Cement Association Skokie.
[3] J. Xiao, C. Qiang, A. Nanni, K. Zhang, Use of sea-sand and seawater in concrete construction: Current status and future opportunities, Constr. Build. Mater. 155 (2017) 1101-1111.
[4] M. Guo, B. Hu, F. Xing, X. Zhou, M. Sun, L. Sui, Y. Zhou, Characterization of the mechanical properties of eco-friendly concrete made with untreated sea sand and seawater based on statistical analysis, Constr. Build. Mater. 234 (2020) 117339.
[5] M. Kummu, J. Guillaume, H. de Moel, S. Eisner, M. Flörke, M. Porkka, S. Siebert, T.I. Veldkamp, P.J. Ward, The world's road to water scarcity: shortage and stress in the 20th century and pathways towards sustainability, Scientific reports 6 (2016) 38495.
[6] O. Bozorg-Haddad, B. Zolghadr-Asli, P. Sarzaeim, M. Aboutalebi, X. Chu, H.A. Loáiciga, Evaluation of water shortage crisis in the Middle East and possible remedies, Journal of Water Supply: Research and Technology—AQUA 69(1) (2020) 85-98.
[7] Z. Chen, Y. Dou, D. Zhao, Desalination and water price management as water shortage strategies: South Africa in 20 years, Fresenius Environmental Bulletin 27(1) (2018) 81-90.
[8] R. Clarke, Water: the international crisis. 2013: Routledge.
[9] A. Witze, Seawater is the secret to long-lasting Roman concrete, Natur (2017)
[10] A.M. Ragab, M.A. Elgammal, O.A. Hodhod, T.E. Ahmed, Evaluation of field concrete deterioration under real conditions of seawater attack, Constr. Build. Mater.

119 (2016) 130-144.
[11] B. Shang, Y. Li, Application feasibility of HRB400 steel in seawater and marine sand concrete, Mater. Corros. 69(10) (2018) 1478-1488.
[12] S. Uthaman, R. George, V. Vishwakarma, M. Harilal, J. Philip, Enhanced seawater corrosion resistance of reinforcement in nanophase modified fly ash concrete, Constr. Build. Mater. 221 (2019) 232-243.
[13] H. Zheng, W. Li, F. Ma, Q. Kong, The performance of a surface-applied corrosion inhibitor for the carbon steel in saturated Ca (OH) 2 solutions, Cem. Concr. Res. 55 (2014) 102-108.
[14] J. Wang, E. Liu, L. Li, Multiscale investigations on hydration mechanisms in seawater OPC paste, Constr. Build. Mater. 191 (2018) 891-903.
[15] T.U. Mohammed, H. Hamada, T. Yamaji, Performance of seawater-mixed concrete in the tidal environment, Cem. Concr. Res. 34(4) (2004) 593-601.
[16] Z.G. Shi, Z.H. Shui, Q. Li, H.N. Geng, Combined effect of metakaolin and sea water on performance and microstructures of concrete, Constr. Build. Mater. 74 (2015) 57-64.
[17] S. Kaushik, S. Islam, Suitability of sea water for mixing structural concrete exposed to a marine environment, Cem. Concr. Compos. 17(3) (1995) 177-185.
[18] T. Nishida, N. Otsuki, H. Ohara, Z.M. Garba-Say, T. Nagata, Some considerations for applicability of seawater as mixing water in concrete, J. Mater. Civ. Eng. 27(7) (2015) B4014004.
[19] F.M. Wegian, Effect of seawater for mixing and curing on structural concrete, The IES Journal Part A: Civil & Structural Engineering 3(4) (2010) 235-243.
[20] M. Etxeberria, J.M. Fernandez, J. Limeira, Secondary aggregates and seawater employment for sustainable concrete dyke blocks production: Case study, Constr. Build. Mater. 113 (2016) 586-595.
[21] A. Younis, U. Ebead, P. Suraneni, A. Nanni, Fresh and hardened properties of seawater-mixed concrete, Constr. Build. Mater. 190 (2018) 276-286.
[22] Y. Sun, C.S. Poon. Effect of Seawater on the Hydration of Tricalcium Silicate. in International RILEM Workshop on Concrete Durability and Service Life Planning (ConcreteLife). 2020. Springer.
[23] M.M. Islam, M.S. Islam, M. Al-Amin, M.M. Islam, Suitability of sea water on curing and compressive strength of structural concrete, Journal of Civil Engineering (IEB) 40(1) (2012) 37-45.
[24] Y. Zhang, Y. Sun, H. Zheng, Y. Cai, W.L. Lam, C.S. Poon, Mechanism of strength evolution of seawater OPC pastes, Advances in Structural Engineering (2021) 1369433221993299.
[25] J.J. Chen, L. Sorelli, M. Vandamme, F.J. Ulm, G. Chanvillard, A Coupled nanoindentation/SEM-EDS study on low water/cement ratio Portland cement paste: evidence for C–S–H/Ca (OH) 2 nanocomposites, J. Am. Ceram. Soc. 93(5) (2010) 1484-1493.
[26] D. Davydov, M. Jirasek, L. Kopecký, Critical aspects of nano-indentation

technique in application to hardened cement paste, Cem. Concr. Res. 41(1) (2011) 20-29.
[27] M.J. DeJong, F.-J. Ulm, The nanogranular behavior of CSH at elevated temperatures (up to 700 C), Cem. Concr. Res. 37(1) (2007) 1-12.
[28] E.M. Foley, J.J. Kim, M.R. Taha, Synthesis and nano-mechanical characterization of calcium-silicate-hydrate (CSH) made with 1.5 CaO/SiO2 mixture, Cem. Concr. Res. 42(9) (2012) 1225-1232.
[29] C. Hu, Z. Li, A review on the mechanical properties of cement-based materials measured by nanoindentation, Constr. Build. Mater. 90 (2015) 80-90.
[30] M.C.G. Juenger, P.J.M. Monteiro, E.M. Gartner, G.P. Denbeaux, A soft X-ray microscope investigation into the effects of calcium chloride on tricalcium silicate hydration, Cem. Concr. Res. 35(1) (2005) 19-25.
[31] J. Cheung, A. Jeknavorian, L. Roberts, D. Silva, Impact of admixtures on the hydration kinetics of Portland cement, Cem. Concr. Res. 41(12) (2011) 1289-1309.
[32] G. Edwards, R. Angstadt, The effect of some soluble inorganic admixtures on the early hydration of portland cement, J. Appl. Chem. 16(5) (1966) 166-168.
[33] X.R. Li, A. Ouzia, K. Scrivener, Laboratory synthesis of C3S on the kilogram scale, Cem. Concr. Res. 108 (2018) 201-207.
[34] M. Miller, C. Bobko, M. Vandamme, F.-J. Ulm, Surface roughness criteria for cement paste nanoindentation, Cem. Concr. Res. 38(4) (2008) 467-476.
[35] K. Scrivener, R. Snellings, B. Lothenbach, A practical guide to microstructural analysis of cementitious materials. 2018: Crc Press.
[36] M. Vandamme, F. Ulm, The nanogranular origin of concrete creep: a nanoindentation investigation of microstructure and fundamental properties of calcium-silicate-hydrates. Vol. 69. 2008.
[37] W. Wilson, J. Rivera-Torres, L. Sorelli, A. Durán-Herrera, A. Tagnit-Hamou, The micromechanical signature of high-volume natural pozzolan concrete by combined statistical nanoindentation and SEM-EDS analyses, Cem. Concr. Res. 91 (2017) 1-12.
[38] N. Singh, V. Singh, S. Rai, S. Chaturvedi, Effect of lignosulfonate, calcium chloride and their mixture on the hydration of RHA-blended Portland cement, Cem. Concr. Res. 32(3) (2002) 387-392.
[39] V. Ramachandran, Accelerators, in Concrete admixtures handbook. 1996, Elsevier. p. 185-285.
[40] S. Abedi, M. Slim, R. Hofmann, T. Bryndzia, F.-J. Ulm, Nanochemo-mechanical signature of organic-rich shales: a coupled indentation–EDX analysis, Acta Geotechnica 11(3) (2016) 559-572.
[41] Z. Luo, W. Li, Y. Gan, K. Mendu, S.P. Shah, Applying grid nanoindentation and maximum likelihood estimation for N-A-S-H gel in geopolymer paste: Investigation and discussion, Cem. Concr. Res. 135 (2020)
[42] H.M. Jennings, J.J. Thomas, J.S. Gevrenov, G. Constantinides, F.-J. Ulm, A multi-technique investigation of the nanoporosity of cement paste, Cem. Concr. Res. 37(3) (2007) 329-336.
[43] V. Kanchanason, J. Plank, Role of pH on the structure, composition and morphology of CSH–PCE nanocomposites and their effect on early strength

development of Portland cement, Cem. Concr. Res. 102 (2017) 90-98.
[44] T. Bach, E. Chabas, I. Pochard, C.C.D. Coumes, J. Haas, F. Frizon, A. Nonat, Retention of alkali ions by hydrated low-pH cements: Mechanism and Na+/K+ selectivity, Cem. Concr. Res. 51 (2013) 14-21.
[45] G. Plusquellec, A. Nonat, Interactions between calcium silicate hydrate (C-S-H) and calcium chloride, bromide and nitrate, Cem. Concr. Res. 90 (2016) 89-96.
[46] E. Bernard, B. Lothenbach, C. Cau-Dit-Coumes, C. Chlique, A. Dauzères, I. Pochard, Magnesium and calcium silicate hydrates, Part I: Investigation of the possible magnesium incorporation in calcium silicate hydrate (C-S-H) and of the calcium in magnesium silicate hydrate (M-S-H), Appl. Geochem. 89 (2018) 229-242.
[47] E. Bernard, B. Lothenbach, F. Le Goff, I. Pochard, A. Dauzères, Effect of magnesium on calcium silicate hydrate (C-S-H), Cem. Concr. Res. 97 (2017) 61-72.
[48] E.P. Barrett, L.G. Joyner, P.P. Halenda, The determination of pore volume and area distributions in porous substances. I. Computations from nitrogen isotherms, J. Am. Chem. Soc. 73(1) (1951) 373-380.
[49] O. Wenzel, M. Schwotzer, E. Müller, V.S.K. Chakravadhanula, T. Scherer, A. Gerdes, Investigating the pore structure of the calcium silicate hydrate phase, Mater. Charact. 133 (2017) 133-137.
[50] H. Lee, R.D. Cody, A.M. Cody, P.G. Spry, Observations on brucite formation and the role of brucite in Iowa highway concrete deterioration, Environmental & Engineering Geoscience 8(2) (2002) 137-145.
[51] E. Bernard, B. Lothenbach, D. Rentsch, I. Pochard, A. Dauzères, Formation of magnesium silicate hydrates (MSH), Physics and Chemistry of the Earth, Parts A/B/C 99 (2017) 142-157.